

Article

Rapid Waste Motor Oil Conversion into Diesel-Range Hydrocarbons Using Hydrochar as Catalyst: Kinetic Study and Product Characterization

Herman A. Murillo ¹, Evelyn Juiña ¹, Karla Vizuete ², Alexis Debut ², Daniel Echeverría ³, Sebastian Taco-Vasquez ³ and Sebastian Ponce ^{1,*}

- ¹ Department of Chemical Engineering, Universidad San Francisco de Quito USFQ, Diego de Robles s/n y Av. Interoceánica, Quito 170901, Ecuador; hmurillo@usfq.edu.ec (H.A.M.); ejuinaj@alumni.usfq.edu.ec (E.J.)
- ² Centro de Nanociencia y Nanotecnología, Universidad de las Fuerzas Armadas ESPE, Av. General Rumiñahui s/n y Ambato, Sangolquí 171103, Ecuador; ksvizuete@espe.edu.ec (K.V.); apdebut@espe.edu.ec (A.D.)
- ³ Department of Chemical Engineering, Escuela Politécnica Nacional, Ladrón de Guevara E11-253, Quito 170525, Ecuador; daniel.echeverria@epn.edu.ec (D.E.); sebastian.taco@epn.edu.ec (S.T.-V.)
- * Correspondence: sponce@usfq.edu.ec

Abstract: Herein, raw and alkali-treated hydrochars from biomass waste are prepared as a highly active catalyst for the conversion of waste motor oil into diesel-like fuels. Among all materials, hydrochar obtained at 250 °C and subsequent alkali activation with KOH showed a 600% improvement of the kinetic constant from 0.0088 to 0.0614 m⁻¹. Conversion values at the same conditions were also improved from 66 to 80% regarding thermal and catalytic cracking, respectively. Moreover, the activation energy was also reduced from 293 to 246 kJ mol⁻¹ for thermal and catalytic cracking, respectively. After characterization, the enhanced catalytic activity was correlated to an increased surface area and functionalization due to the alkali activation. Finally, the liquid product characterization demonstrated that catalytic cracking is more effective than thermal cracking for producing hydrocarbons in the diesel range. In particular, hydrochar-based catalysts are suggested to promote the formation of specific hydrocarbons so that the carbon distribution can be tailored by modifying the hydrothermal treatment temperature.

Keywords: hydrochar; catalysis; waste motor oil; chemical recycling; diesel-like fuel



Citation: Murillo, H.A.; Juiña, E.; Vizuete, K.; Debut, A.; Echeverría, D.; Taco-Vasquez, S.; Ponce, S. Rapid Waste Motor Oil Conversion into Diesel-Range Hydrocarbons Using Hydrochar as Catalyst: Kinetic Study and Product Characterization.

Recycling **2024**, *9*, 39. <https://doi.org/10.3390/recycling9030039>

Academic Editor: Salustiano Mato De La Iglesia

Received: 15 March 2024

Revised: 25 April 2024

Accepted: 4 May 2024

Published: 17 May 2024



Copyright: © 2024 by the authors. Licensee MDPI, Basel, Switzerland. This article is an open access article distributed under the terms and conditions of the Creative Commons Attribution (CC BY) license (<https://creativecommons.org/licenses/by/4.0/>).

1. Introduction

Hydrochar is a carbonaceous material prepared through hydrothermal carbonization (HTC), showing various applications in different fields, including agriculture, crop improvement, wastewater treatment, carbon sequestration, and energy production [1–4]. Due to the possibility of modifying its physicochemical properties (e.g., by physical or chemical activation, metal doping, among other processes) to enhance its sorption potential, hydrochar is employed as a heterogeneous catalyst material. In this sense, physical or chemical activation methods can develop the production of highly porous carbons. Particularly, chemical activation techniques have been explored to enhance the adsorption capacity and catalytic activity of hydrochar. Acid (e.g., phosphoric acid) or alkaline solutions (e.g., NaOH, KOH) are commonly used for this particular purpose [5,6]. It allows volatile matter removal, increasing the presence of oxygenated functional groups, thus improving surface area and functionalization. This can also be upgraded by incorporating metals over the hydrochar surface [3,6]. The hydrochar-as-catalyst concept includes applications in 5-HMF production [7], hydrogen-rich syngas [8], and biofuels [9]. Nevertheless, there are still other reactions to be explored. In this sense, hydrochar-based catalysts have not been used for waste motor oil (WMO) cracking.

WMO is a critical problem of modern society since it contributes significantly to environmental pollution. It is often discarded improperly, leading to soil and water contamination. In this sense, several recycling techniques have been developed to convert WMO into valuable products. Among pyrolysis and co-pyrolysis, cracking is a promising technique for producing secondary diesel-like fuels (DLF) from WMO [10–13]. Regarding the latter, our research group demonstrated that mesoporous aluminum silicates work as effective catalysts for WMO cracking into DLF, with Ni-doped Al/Si showing outstanding catalytic activity. Metal-doped Al/Si catalysts positively impacted cracking reactions despite reduced surface area. Among them, Ni-doped basic Al/Si exhibited three times higher conversions and yields than metal-free counterparts [14,15]. Recently, chemically activated rice husk biochar (RH-KOH) was applied to replace synthetic materials with biomass-based catalysts, outperforming previous synthetic materials and implying lower activation energy [16]. Hence, following the trend in thermochemical conversion processes, hydrochar is a suitable alternative for larger-scale applications. This is due to lower energy consumption when performing HTC [17] ranging from 180 to 250 °C under subcritical water [18]. Yet, when conducting pyrolysis to produce biochar, the reaction temperatures may reach 900 °C in some cases [19]. Although HTC is less severe in biomass decomposition than pyrolysis, hydrothermal processing bestows interesting properties to the solid product. Energy densification on hydrochar may seem lower; however, other properties like surface functionalization with oxygenated groups make this novel material set to be used as a catalyst for specific applications. It includes calcium-enriched hydrochar for glucose isomerization, hydrogen production using algal-derived hydrochar, and functionalized hydrochar for biodiesel generation, among others [20–22], making it attractive for WMO cracking.

In summary, this study explores the novel application of non-treated and alkali-treated hydrochar derived from rice husk as catalysts for WMO cracking in a batch reactor. A first approach addresses the kinetic study of the hydrochar-assisted WMO cracking, including the determination of kinetic parameters such as reaction order, kinetic constant, and activation energy. The aim is to first realize the hydrochar behavior and then the effect of the alkali treatment on this cracking process. On the other hand, a complete material characterization via FTIR, single-point BET surface area analysis, XRD, SEM, and EDS was conducted to fully understand the potential use of hydrochar as a catalyst. Furthermore, in order to assess the hydrochar catalytic activity, the liquid products resulting from thermal (i.e., without catalyst) and catalytic cracking were characterized via GC-MS. A comparison to commercial diesel was also established to find the resemblance of the obtained DLF in this work to commercial samples in terms of chemical composition and calorific values.

Based on this background, it is crucial to acknowledge that an in-depth investigation of the catalytic properties of hydrochar will not only provide useful insights for WMO conversion but also for other catalyzed reactions, opening up further alternatives for subsequent studies. Valorizing residual biomass, to treat another residue such as WMO, promotes a comprehensive approach regarding circular economy, where residues are upgraded to valuable products with particular attention on the development of the hydrochar-as-catalyst concept.

2. Results and Discussion

2.1. Catalytic Cracking of WMO and Kinetic Study

Rice husk was chosen as a raw material for hydrochar production and used for the catalytic cracking of WMO. In a previous contribution, biochar alkali treatment remarkably influenced the kinetic constant for WMO cracking [16]. Thus, in this study, hydrochars were alkali-treated with KOH to test the activation influence on the material's morphology and performance.

In a typical experiment, the reaction starts after a 15-min heating period until the temperature reaches a constant value (see Figure S1 in the Supplementary Data). After this period, the liquid product recovery begins. The reaction continues until the recovery of the liquid product stops. Then, gases and solid residues are weighted for calculations.

Solid residues combine solid catalysts and by-products of hydrocarbon decomposition named coke. Figure 1a compares the WMO conversion as a function of time in a thermal and a catalytic cracking reaction, showing that a catalytic reaction allows for higher conversions. For instance, 67% and 75% of conversion are obtained for thermal and catalytic (175_HKOH) cracking, respectively (please refer to Figure S2 in the Supplementary Data for the conversion and kinetic plots of the other catalysts). Table 1 shows the conversion values for all tested catalysts in this study. It is well known that the conversion increase can be attributed to decreased coke and other gas formation while increasing the production of desired compounds, such as iso-paraffin [23], due to a catalyst.

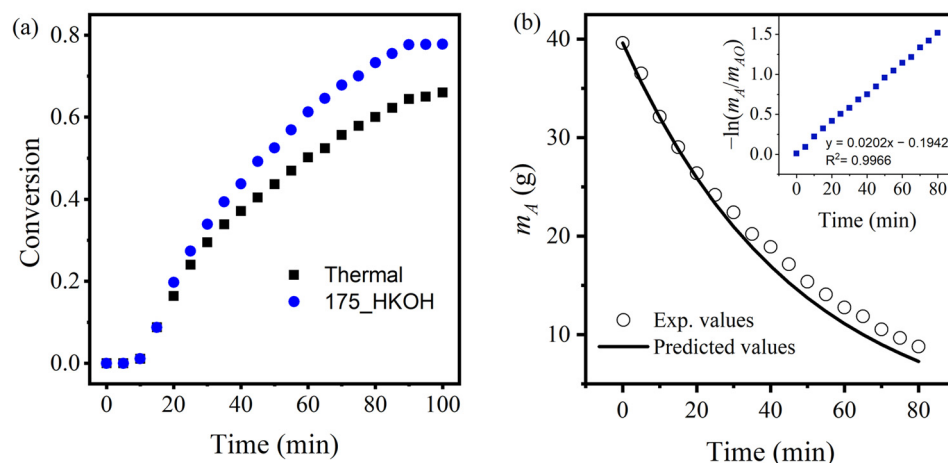


Figure 1. (a) Exemplarily conversion vs. time curves of the thermal and catalytic cracking of WMO, and (b) experimental and predicted curves. Inset: kinetic constant calculation. Reaction conditions: temperature: 420 °C, 40 g of WMO, and 0 and 0.4 wt% of catalyst (175_HKOH).

Table 1. Conversion and kinetic constants for cracking experiments conducted at 420 °C.

| Catalyst | Conversion (%) | k (min ⁻¹) | k_{rel} |
|-------------------------------------|----------------|----------------------------------|-----------|
| Thermal cracking (without catalyst) | 66.85 ± 1.78 | 0.0088 ± 2.8 × 10 ⁻⁴ | 1.00 |
| 175_H | 75.79 ± 2.46 | 0.0206 ± 1.2 × 10 ⁻³ | 2.34 |
| 175_HKOH | 74.96 ± 3.84 | 0.0223 ± 1.5 × 10 ⁻³ | 2.53 |
| 200_H | 73.69 ± 0.84 | 0.0153 ± 1.8 × 10 ⁻³ | 1.74 |
| 225_H | 74.02 ± 6.44 | 0.0156 ± 4.9 × 10 ⁻⁴ | 1.77 |
| 250_H | 73.41 ± 7.16 | 0.0182 ± 3.7 × 10 ⁻³ | 2.07 |
| 250_HKOH | 80.41 ± 6.61 | 0.0614 ± 1.01 × 10 ⁻² | 6.98 |
| Al/Si + Zn * | 84 | 0.0159 | 1.8 |
| RH-KOH * | 86 | 0.0249 | 2.8 |

* Previously reported materials [16].

The differential method obtained the kinetic constant in all cracking catalytic reactions. Figure 1b shows an example of the linearized form of the potential law model, which is modeled by a linear equation. The thermal and cracking catalytic reactions have a pseudo-first-order mechanism, which was expected from previous contributions [15,16].

Table 1 and Figure 1 summarize the kinetic constants calculated for each material synthesized in this study. First, hydrochars prepared at different HTC temperatures were used in the catalytic cracking of WMO. The obtained kinetic constants in thermal cracking and catalytic cracking are compared. It is observed that compared to thermal cracking, the kinetic constants using hydrochar have a considerable increase (around two times higher). Interestingly, there is no appreciable difference among materials prepared at different temperatures (175, 200, 225, and 250 °C). Remarkably, raw hydrochars surpass the kinetic constants previously reported for synthetic materials (i.e., Al/Si + Zn) and show comparable kinetic constants to alkali-treated biochars reported recently by Rodriguez et al. [16] at

the same operation conditions. Conversion values seem not to be affected as well. The same study demonstrated that alkali treatment improves the biochar's surface area and surface functionalization for WMO catalytic cracking. Thus, 175_H and 250_H hydrochars were KOH treated and tested. Unpredictably, alkali-treated hydrochars carbonized at 175 °C (175_HKOH) do not significantly increase the kinetic constant. However, for alkali-treated hydrochars carbonized at 250 °C (250_HKOH), a surprising increment of the kinetic constant is observed (around seven times higher than the thermal cracking process) being so far the most active material for the chemical recycling of WMO.

In addition to evaluating the catalytic behavior of the materials, it is crucial to consider the mass yield, which represents the amount of hydrochar produced relative to the initial feedstock. The mass yield percentages for all tested materials are depicted in Figure 2a. As mentioned above, the raw hydrochars exhibit comparable kinetic constants to previously reported biochars. However, the mass yields of hydrochar surpass those from biochar (below 20%), which might be an important factor for a possible process scaling up. At this point, it must be mentioned that the alkali treatment decreased the solid yield significantly: ~30% for the 175_HKOH catalyst and ~20% for the 250_HKOH catalyst.

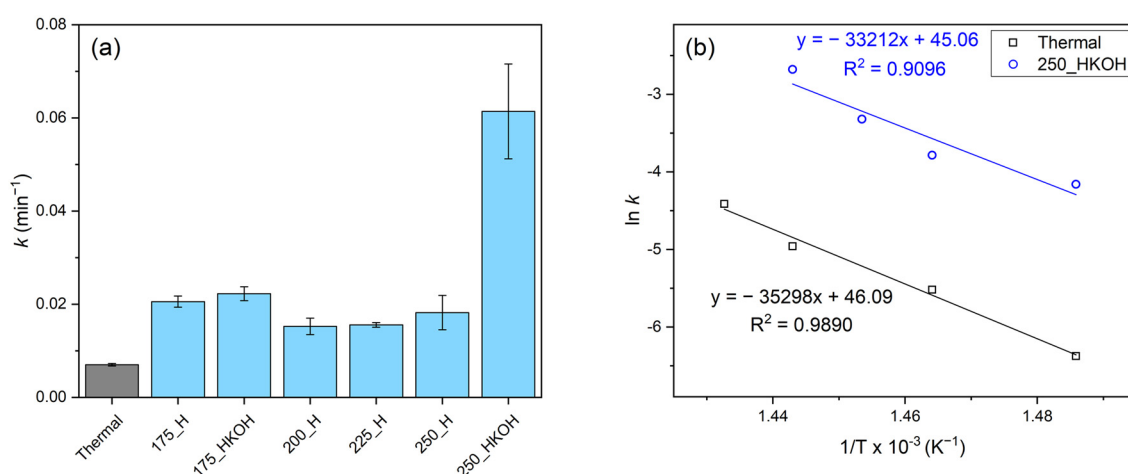


Figure 2. (a) Obtained kinetic constants for waste motor oil in thermal and catalytic cracking. (b) Kinetic analysis: Arrhenius plot for WMO's thermal and catalytic (250_HKOH) cracking. Reaction conditions: temperature: 420 °C, 40 g of WMO, and 0.4 wt% of catalyst.

Remarkably, the 250_HKOH samples exhibit similar mass yields to biochar but with kinetic constants three times higher. This analysis unequivocally demonstrates that hydrochar is a more economically viable material for recycling motor oil on a larger scale.

A complete kinetic analysis was conducted using the best catalyst (250_HKOH) compared with the thermal cracking (see Table 2 and Figure 2b). The kinetic constants were calculated at four different temperatures (i.e., 400, 410, 420, and 425 °C). A linear dependence was expected between the kinetic constants and the temperature for the Arrhenius equation, so the activation energy was obtained, E_a , and the pre-exponential factor, k_0 . A considerable reduction is observed for the catalytic compared to the thermal cracking (276.12 to 293.48 kJ mol⁻¹), respectively.

Finally, in the literature, most studies generate DLF through pyrolysis and co-pyrolysis, often involving incorporating various residues such as polymers and surgical masks [13,24] (see Table 3). These methods typically demand more significant energy inputs than the cracking process, which might be developed at lower temperatures with the presence of a catalyst. However, in the context of the cracking method, the material developed in this study outperforms previous efforts, offering the distinct advantage of utilizing a material synthesized via HTC at lower temperatures and costs.

Table 2. Kinetic parameters obtained from the waste motor oil thermal and catalytic cracking.

| Catalyst | Temperature (°C) | Kinetic Parameters | | | |
|--|------------------|---------------------------------|----------------------------|-------------------------------|--------|
| | | k (min ⁻¹) | k_0 (min ⁻¹) | E_a (kJ mol ⁻¹) | R^2 |
| Thermal cracking (without catalyst) | 400 | $0.0017 \pm 1.4 \times 10^{-4}$ | 1.04×10^{20} | 293.48 | 0.9890 |
| | 410 | $0.0040 \pm 4.6 \times 10^{-4}$ | | | |
| | 420 | $0.0070 \pm 4.2 \times 10^{-4}$ | | | |
| | 425 | $0.0121 \pm 2.0 \times 10^{-4}$ | | | |
| 250_HKOH | 400 | $0.0156 \pm 8.5 \times 10^{-4}$ | 3.69×10^{19} | 276.12 | 0.9096 |
| | 410 | $0.0227 \pm 4.4 \times 10^{-3}$ | | | |
| | 415 | $0.0361 \pm 7.8 \times 10^{-4}$ | | | |
| | 420 | $0.0686 \pm 4.2 \times 10^{-3}$ | | | |

Table 3. Summary of literature dealing with waste motor oil recycling.

| Recycling Method | Feedstock | Conditions | Target Product | Kinetic Constant (min ⁻¹) | Ref. |
|--------------------|-----------------------------------|-----------------------------|----------------|---------------------------------------|------------|
| Co-pyrolysis | WMO + Tetra pack | 500 °C Fixed bed reactor | Diesel | NA | [13] |
| Co-pyrolysis | WMO + Surgical mask/Woody biomass | 400 °C Batch reactor | Diesel | NA | [24] |
| Gasification | WMO | 800–1200 °C | Syngas | NA | [10] |
| Co-pyrolysis | LDPE | 650 °C | Diesel | NA | [25] |
| Catalytic cracking | WMO + AlSi-Zn catalyst | 420 °C | Diesel | 0.0159 | [15] |
| Catalytic cracking | WMO + alkali-biochar catalyst | 420 °C | Diesel | 0.0249 | [16] |
| Catalytic cracking | WMO + 250H_KOH catalyst | 420 °C | Diesel | 0.0614 | This study |

2.2. Hydrochar Catalyst Characterization

Material characterization was developed to obtain insights into the catalytic behavior. Morphological changes were studied for non- and alkali-treated 175_H and 250_H hydrochars. For hydrochar obtained at 175 °C (Figure 3a), pores are hardly observed at the material's surface (i.e., low specific surface area-SSA $\sim 4.25 \text{ m}^2 \text{ g}^{-1}$), while at 250 °C (Figure 3c), an evident carbonization effect is observed (SSA $\sim 19.83 \text{ m}^2 \text{ g}^{-1}$). The formation of porosity is related to the higher degree of biomass degradation at higher temperatures during HTC. Even though there was an apparent increase in porosity at higher carbonization temperatures, an evident effect in the catalytic behavior was not observed, as discussed in the previous section. As expected, after alkali activation, many cavities on the hydrochar surface are displayed (Figure 3b,d). It is known that organic material and silica were removed due to alkali treatment unblocking the pores, increasing the specific surface area (e.g., from ~ 19.83 to $110.67 \text{ m}^2 \text{ g}^{-1}$ for 250_H and 250_HKOH, respectively). Ash content measurements of raw biomass and hydrochars before and after alkali treatment were developed. A higher ash content of 250_HKOH ($\sim 44 \text{ wt}\%$) compared to 250_H ($\sim 39 \text{ wt}\%$) and raw biomass ($\sim 19 \text{ wt}\%$) is obtained, which might be evidence of a higher degree of degradation of organic material followed by hydrolysis and alkali treatment. This higher presence of inorganic material at the material's surface might contribute to its superior catalytic activity.

For further evidence, an EDS analysis of the materials was conducted. After alkali treatment, two effects are observed (see Figure 3e). First, the lower presence of silica in alkali-treated materials is confirmed (e.g., from ~ 25 to $8 \text{ normalized wt}\%$ for 250_H and 250_HKOH, respectively). Moreover, the potassium and oxygen content increases, which might imply that KOH activation was scattered over the hydrochar surface. The latter can be related to the presence of more basic sites, which are known to be more active for WMO cracking. Thus, due to alkali treatment, the excellent activity of 250_HKOH might be related to both the high specific surface area and surface functionalization.

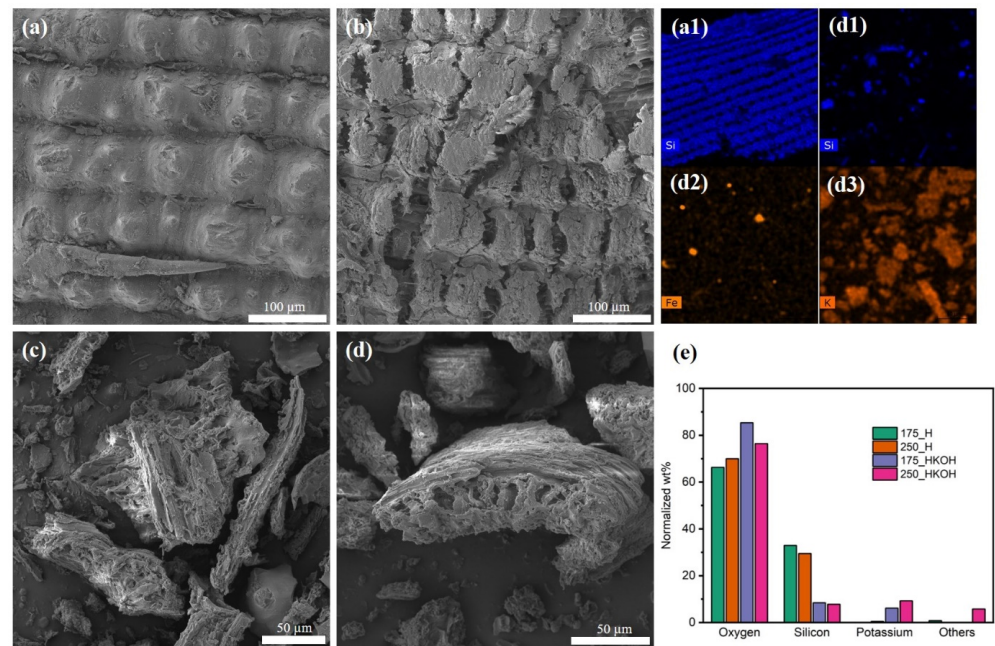


Figure 3. SEM images of (a) 175_H, (b) 175_HKOH, (c) 250_H, (d) 250_HKOH, and (e) elementary normalized wt% from EDS. Inset: EDS map showing the spectral image of (a1) Si in 175_H, (d1) Si, (d2) Fe, and (d3) K in 250_HKOH.

For further evidence, FTIR and XRD analyses were carried out (see Figure 4). FTIR spectra show typical peaks for rice husk after carbonization. Functional groups such as O-H (3400 and 1625 cm^{-1}), C=H (between 2850 and 3000 cm^{-1}), C=O (around 1710 cm^{-1}), and C=C (around 1625 cm^{-1}) [26–28] are observed, which become more intense at higher carbonization temperatures and after treatment. Moreover, typical for rice husks, a peak between 1100 and 1000 cm^{-1} corresponds to Si-O-Si, following the high silica content of rice husks. Interestingly, as expected from the previous characterization, this peak tends to reduce intensity after the alkali treatment.

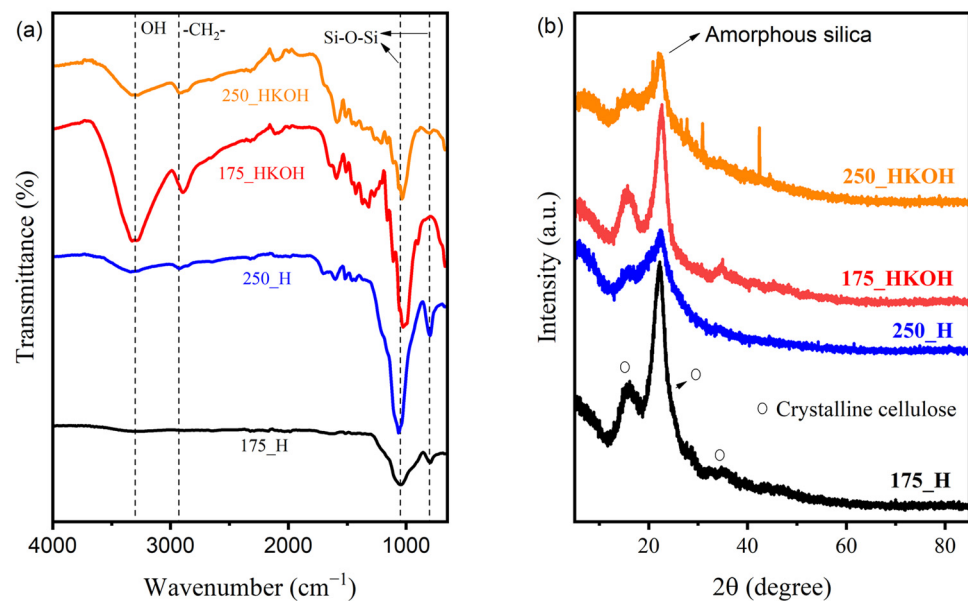


Figure 4. Hydrochar characterization: (a) FTIR spectra, and (b) X-ray diffractogram.

From XRD spectra, it is clearly observable that there is still a high degree of crystallization for non-and treated hydrochars carbonized at $175\text{ }^\circ\text{C}$. Characteristics peaks

at $2\theta = 15, 22.5^\circ$ commonly related to cellulose are detected. However, for 250_H and 250_HKOH, a higher degree of carbonization is obtained with the spectra resembling a carbonaceous amorphous material in accordance with the higher degradation. Interestingly, for 250_HKOH, due to the degradation degree after the alkali treatment, new sharp peaks are detected, which might be related to the detection of other metals present in rice husk that might become available and might increase the catalytic activity of 250_HKOH. This behavior is also confirmed via EDS mapping, where the exemplary presence of Si, Fe, and K are represented in Figure 3(d1,d3) compared to solely Si in hydrochar before treatment (Figure 3d(a1)), which is accordance with the increment of ash content in the 250_HKOH.

In addition to evaluating the catalytic behavior of the materials, it is crucial to consider the mass yield, which represents the amount of hydrochar produced relative to the initial feedstock as well as the mass remaining after the alkali treatment. The mass yield percentages for all tested materials are depicted in Figure 5. Most of the hydrochars surpass the mass yields from biochar (<20%), which might be an important factor for a possible process scaling up. Also, it must be mentioned that the alkali treatment decreased the solid yield significantly: ~30% for the 175_HKOH catalyst and ~20% for the 250_HKOH catalyst.

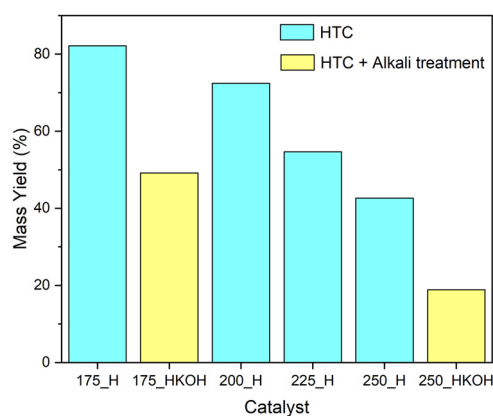


Figure 5. Mass yield values for the studied catalysts.

2.3. DLF Characterization

To fully understand the catalytic effect on the cracking products, DLF samples from thermal and catalytic cracking with the 175_HKOH and 250_HKOH catalysts were characterized via GC-MS. Commercial diesel was also studied to determine the DLF's resemblance to commercial samples. For instance, the highest abundance peaks of DLF from thermal cracking were attained at pretty low retention times regarding commercial diesel, reflecting the presence of many low-molecular-weight hydrocarbons (as indicated in Figure S3 in the Supplementary Data). Thermal cracking seemed more likely to break down hydrocarbon chains into smaller fragments. However, notable peaks were also observed at mid and high retention times. Notice that based on the average carbon numbers (ACN) presented in Figure 6a,b (i.e., 15.8 and 15.6, for commercial diesel and DLF from thermal cracking, respectively), the thermal-DLF resembles commercial diesel including significant concentrations of isoparaffins but higher naphthene levels for thermal-cracking DLF. Yet, the carbon distribution from thermal processing appears to be more heterogeneous, where similar hydrocarbon concentrations can be identified in different zones of the carbon number classification. Conversely, a few hydrocarbon fractions account for most of the commercial diesel composition: C13, C15, C16, and C21.

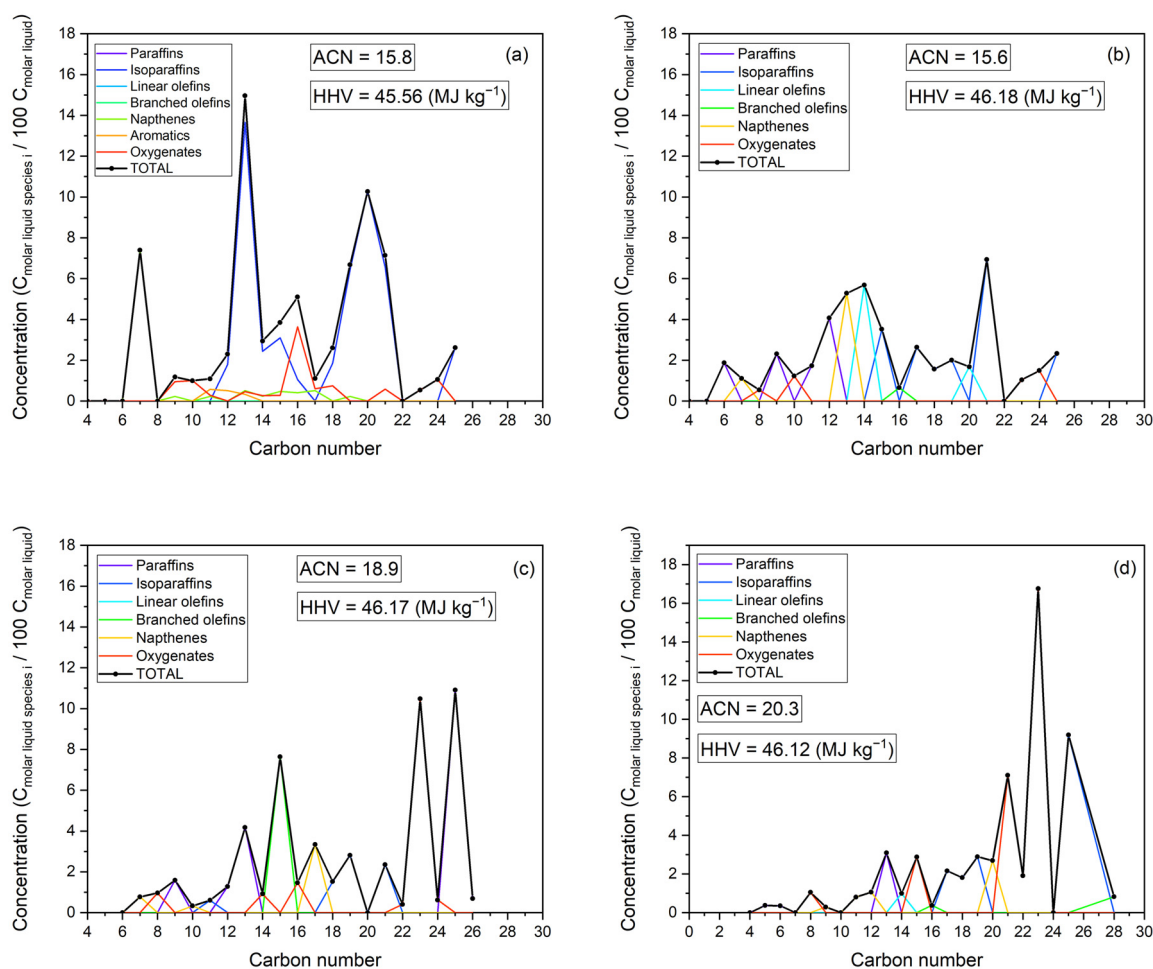


Figure 6. Carbon distribution: (a) commercial diesel, (b) DLF from thermal cracking, (c) DLF from 175_HKOH, and (d) DLF from 250_HKOH.

On the other hand, the abundance peaks from catalytic cracking in both cases concentrate at higher retention times, surpassing those from commercial diesel, as also observed in Figure S4. Likewise, some light hydrocarbons remain in the liquid fraction but to a lesser extent. This is an improvement by the catalytic cracking compared to the thermal in the sense lighter hydrocarbons were decreased, and more hydrocarbons remained in the diesel range (\sim C12 to C22) [29]. Still, some peaks at low retention times persisted when using the 175_HKOH catalyst, but this issue was addressed by employing the 250_HKOH catalyst, which partially reduced the abundance of these peaks. This is confirmed by referring to Figure 6c,d, where low-carbon-number peaks (e.g., C4 to C10) are broader for the DLF using 175_HKOH compared to 250_HKOH. Remarkably, it seems the carbon distribution can be tailored by increasing the HTC temperature for catalyst preparation toward reducing these light hydrocarbons.

The highest ACN showed by the 250_HKOH-assisted cracking (CAN = 20.3, still in the diesel range) supports the explanation given above regarding this hydrochar producing heavier hydrocarbons with little fractions surpassing the diesel range. Nevertheless, this behavior was found in commercial diesel, too, since it reflected an ACN of 15.8 but included little fractions out of the diesel range [30]. The main difference lies in the fact that $>$ C22 hydrocarbons prevailed in DLF samples from hydrochar-assisted catalytic cracking. In this context, although thermal cracking produced a DLF with an ACN close to commercial diesel, the hydrocarbon concentrations were lower compared to commercial diesel and catalytic-cracking DLF samples. This is definitely an advantage shown by the catalytic process. Regarding hydrocarbon types, paraffins and oxygenates prevailed in DLF using

175_HKOH, but when using 250_HKOH, paraffins were partially reduced, and isoparaffins prevailed alongside oxygenates. Although the presence of oxygenates in diesel fuels may decrease their calorific value, favorable effects have also been observed during combustion, especially in reducing exhaust emissions [31]. Finally, according to the HHV, all DLF samples from both thermal and catalytic cracking showed no significant difference compared to commercial diesel.

3. Materials and Methods

3.1. Hydrochar Preparation

The waste motor oil was provided by a collection station from Quito, Ecuador. Rice husks were obtained from a local market. The reagent for hydrochar activation was potassium hydroxide (KOH).

3.2. Hydrochar Preparation and Alkali Treatment

The hydrothermal treatment was conducted in a 500 mL high-pressure reactor with magnetic stirring (model TGYF-B-500ML, Zheng Zhou, China). In a typical HTC experiment, rice husk and distilled water are loaded based on the operating dry biomass/water ratio (1:20), and then the reactor is closed. The reaction temperature is set at the operating reaction temperature (e.g., 175, 200, 225, and 250 °C), showing a maximum variation of ± 1 °C. A fixed reaction time of 60 min was set up once the reaction temperature was reached, and a stirring of 1000 rpm was kept during the HTC run. The pressure can vary between 1 and 5 MPa depending on the operating temperature. Once the reaction was finished, the reactor was cooled down at room temperature before being opened, and the hydrochar/process water mixture was separated by vacuum filtration: the filtrate represents the process water, while the material retained in the filter is the hydrochar, which is then dried before subsequent characterization and processing. Before the reactor was opened, the gas phase was purged to alleviate the pressure inside the reactor.

Additionally, 2 g of hydrochar was mixed with 500 mL of a 3 M-KOH solution for alkali treatment. The mixture was stirred at 600 rpm and heated (70 °C) for two hours. Non-activated and alkali-treated hydrochars were dried at 105 °C overnight and then stored for characterization and utilization.

3.3. Experimental Setup for Catalytic Cracking of WMO and Kinetic Analysis

Before the cracking experiments, the collected WMO underwent a pretreatment to remove water and solid residues. WMO went through a metallic mesh (~1 mm) and was then stirred at 50 rpm for 24 h at 115 °C. A Precision Scientific Petroleum Herzog distiller (see Figure S4 in the Supplementary Data) was used for the cracking, including a maximum power of 1100 W. More details on this equipment can be found in our previous study [16]. For the cracking process, 40 g (~45.7 mL) of the pretreated WMO was added into a 250 mL flask, including a 0.4 wt%-catalyst addition. Once the flask was placed into the distiller, it was pre-heated for 10 min at 260 °C and then set to the desired temperature for one minute (420 ± 1 °C).

The studied samples are labeled as T_H, where T represents the HTC temperature, and H means hydrochar (e.g., 175_H refers to the hydrochar obtained at 175 °C). On the other hand, the alkali-activated samples are labeled based on T_HKOH (e.g., 175_HKOH refers to the hydrochar obtained at 175 °C with subsequent alkali activation using KOH).

WMO shows a complex hydrocarbon composition, so the system was streamlined to an average C₃₀-hydrocarbon oil molecule, as previously presented by Vargas et al. [15] and Rodriguez et al. [16] and also indicated by Equation (1). It entails the desired liquid products (i.e., 2P) between C₈ and C₂₀ hydrocarbons are produced using when treating WMO. Additionally, lighter fractions/gaseous fractions are produced (up to C₇) (i.e., B), as presented in Equation (2).





The above model was established according to the mass balance for the distiller. Equation (3) represents the consumption rate of WMO, where n is the reaction order, and k (min^{-1}) is the kinetic constant. These kinetic parameters were attained by means of the differential and integral methods, respectively.

$$R_A = -k \cdot m_A^n \quad (3)$$

The activation energy, E_a (J mol^{-1}), and the pre-exponential factor, k_o (min^{-1}), were calculated according to Arrhenius's law (Equation (4)), where R reflects the universal gas constant, while T represents the temperature expressed in (K).

$$\ln(k) = \ln(k_o) - \frac{E_a}{RT} \quad (4)$$

In order to fully understand the reaction behavior with time, Equation (5) was employed, where V_R refers to the cumulative condensate volume during the reaction, and V_o refers to the initial volume used in the reaction, which are both expressed in mL.

$$X_A = \frac{V_R}{V_o} \quad (5)$$

3.4. Analytical Methods for Hydrochar and DLF Characterization

Hydrochar morphology was analyzed using a Tescan Mira 3 Scanning Electron Microscope (SEM) equipped with a Schottky Field Emission Gun (Brno, Czech Republic). In this case, hydrochar samples were placed on SEM stubs, while a Quorum Q150R ES sputtering evaporator was used to cover the samples with a gold layer of 20 nm (99.99% purity). Energy-Dispersive Spectroscopy (EDS) was also used at 30 kV with a Bruker X-Flash 6 | 30 detector (Billerica, MA, USA) for subsequent elemental analysis. The samples were placed on a stub and covered in duplicate carbon-conductive tape layers. A single-point BET surface area analysis was performed in a Micromeritics' AutoChem II Chemisorption Analyzer (Norcross, GA, USA). The FTIR spectroscopy was carried out using an Agilent Technologies Cary 630 FTIR Spectrometer (Santa Clara, CA, USA) at a 600–4000 cm^{-1} wavenumber range. In this sense, the samples were heated from 25 °C to 900 °C at 10 °C min^{-1} under N_2 atmosphere. The crystallographic structure was determined by X-Ray Diffractometry (XRD) employing a PANalytical Empyrean diffractometer (Malvern, UK) operating at a θ -2 θ configuration of 40 kV and 40 mV.

Furthermore, the DLF chemical composition was determined using a Perkin Elmer Clarus 590 gas chromatograph (Shelton, CT, USA) coupled to a Clarus SQ8S mass spectrometer (GC-MS). The measurement protocol includes the liquid fraction to be cooled at 0 °C so that all hydrocarbons ($\geq \text{C}_5$) can remain in a liquid phase. In addition, calorific values, specifically higher heating values (HHVs), were determined using a Parr Instrument 6400 bomb calorimeter (Moline, IL, USA) based on the ASTM D 4809 standard [32].

4. Conclusions

This work demonstrates activated hydrochars from rice husk as promising materials for the catalytic cracking of waste motor oil. Hydrochars without treatment performed similarly to previously reported materials (synthetic alumina silicates and rice husk biochar). A remarkable increment of the kinetic constant and reduced activation energy was observed with the 250_HKOH catalyst with 600% increment and 20% decrement, respectively. Alkali treatment proved efficient for extracting silica from hydrochar matrix and surface functionalization, while increasing the ash content of the material and thus improving its catalytic activity. By catalytic cracking, the ACN can be tailored to heavier hydrocarbons compared to DLF from thermal cracking, resulting in fuels with a higher concentrated carbon distribution, which is desirable for improved combustion performance. Overall, this study shows

the potential of hydrochars as green catalysts for producing an alternative to commercial diesel. However, developing efficient regeneration methods to restore catalyst activity and reusability is crucial for widespread adoption in large-scale processes. Our future research will be focused on investigating and optimizing such regeneration techniques.

Supplementary Materials: The following supporting information can be downloaded at <https://www.mdpi.com/article/10.3390/recycling9030039/s1>, Figure S1: Exemplary temperature and volume of condensate vs. time curves during thermal cracking of WMO. Reaction conditions: Temperature: 420 °C, 40 g of WMO, 0.4 wt% of catalyst. Figure S2: Conversion vs. time curves for 175_H, 200_H, 225_H, 250_H, and 250_HKOH catalysts. Inset plots: kinetic constant calculation. Figure S3: GC-MS chromatograms: (a) commercial diesel, (b) DLF from thermal cracking, (c) DLF from 175_HKOH, and (d) DLF from 250_HKOH. Figure S4: Picture of the cracking setup used in this study.

Author Contributions: H.A.M.: Conceptualization, Methodology, Investigation, Writing—original draft; E.J.: Investigation, Visualization, Writing—original draft; K.V.: Investigation, Formal analysis; A.D.: Investigation, Writing—review; D.E.: Investigation, Formal analysis; S.T.-V.: Investigation, Formal analysis, and S.P.: Conceptualization, Methodology, Writing—review and editing, Funding acquisition. All authors have read and agreed to the published version of the manuscript.

Funding: The Collaboration Grant (23180) and the Poligrant (24255) programs from Universidad San Francisco de Quito USFQ have supported this research.

Data Availability Statement: The data presented in this study are within the document and the Supplementary Data.

Conflicts of Interest: The authors declare no conflicts of interest.

References

1. Murillo, H.A.; Pagés-Díaz, J.; Díaz-Robles, L.A.; Vallejo, F.; Huiliñir, C. Valorization of Oat Husk by Hydrothermal Carbonization: Optimization of Process Parameters and Anaerobic Digestion of Spent Liquors. *Bioresour. Technol.* **2022**, *343*, 126112. [[CrossRef](#)]
2. Xia, Y.; Yang, T.; Zhu, N.; Li, D.; Chen, Z.; Lang, Q.; Liu, Z.; Jiao, W. Enhanced Adsorption of Pb(II) onto Modified Hydrochar: Modeling and Mechanism Analysis. *Bioresour. Technol.* **2019**, *288*, 121593. [[CrossRef](#)] [[PubMed](#)]
3. Masoumi, S.; Borugadda, V.B.; Nanda, S.; Dalai, A.K. Hydrochar: A Review on Its Production Technologies and Applications. *Catalysts* **2021**, *11*, 939. [[CrossRef](#)]
4. Zhang, Z.; Yang, J.; Qian, J.; Zhao, Y.; Wang, T.; Zhai, Y. Biowaste Hydrothermal Carbonization for Hydrochar Valorization: Skeleton Structure, Conversion Pathways and Clean Biofuel Applications. *Bioresour. Technol.* **2021**, *324*, 124686. [[CrossRef](#)] [[PubMed](#)]
5. Sulaiman, N.S.; Hashim, R.; Mohamad Amini, M.H.; Danish, M.; Sulaiman, O. Optimization of Activated Carbon Preparation from Cassava Stem Using Response Surface Methodology on Surface Area and Yield. *J. Clean. Prod.* **2018**, *198*, 1422–1430. [[CrossRef](#)]
6. Shen, R.; Lu, J.; Yao, Z.; Zhao, L.; Wu, Y. The Hydrochar Activation and Biocrude Upgrading from Hydrothermal Treatment of Lignocellulosic Biomass. *Bioresour. Technol.* **2021**, *342*, 125914. [[CrossRef](#)] [[PubMed](#)]
7. Kang, S.; Ye, J.; Zhang, Y.; Chang, J. Preparation of Biomass Hydrochar Derived Sulfonated Catalysts and Their Catalytic Effects for 5-Hydroxymethylfurfural Production. *RSC Adv.* **2013**, *3*, 7360–7366. [[CrossRef](#)]
8. Gai, C.; Zhang, F.; Guo, Y.; Peng, N.; Liu, T.; Lang, Q.; Xia, Y.; Liu, Z. Hydrochar-Supported, in Situ-Generated Nickel Nanoparticles for Sorption-Enhanced Catalytic Gasification of Sewage Sludge. *ACS Sustain. Chem. Eng.* **2017**, *5*, 7613–7622. [[CrossRef](#)]
9. Norouzi, O.; Heidari, M.; Martinez, M.; Dutta, A. New Insights for the Future Design of Composites Composed of Hydrochar and Zeolite for Developing Advanced Biofuels from Cranberry Pomace. *Energies* **2020**, *13*, 6600. [[CrossRef](#)]
10. Mishra, A.; Siddiqi, H.; Kumari, U.; Behera, I.D.; Mukherjee, S.; Meikap, B.C. Pyrolysis of Waste Lubricating Oil/Waste Motor Oil to Generate High-Grade Fuel Oil: A Comprehensive Review. *Renew. Sustain. Energy Rev.* **2021**, *150*, 111446. [[CrossRef](#)]
11. Maceiras, R.; Alfonsín, V.; Morales, F.J. Recycling of Waste Engine Oil for Diesel Production. *Waste Manag.* **2017**, *60*, 351–356. [[CrossRef](#)]
12. Sarkar, S.; Datta, D.; Deepak, K.S.; Mondal, B.K.; Das, B. Comprehensive Investigation of Various Re-Refining Technologies of Used Lubricating Oil: A Review. *J. Mater. Cycles Waste Manag.* **2023**, *25*, 1935–1965. [[CrossRef](#)]
13. Tekin, K.; Ucar, S.; Karagöz, S. Influence of Co-Pyrolysis of Waste Tetra Pak with Waste Motor Oil on Product Distribution and Properties for Fuel Application. *Energy Fuels* **2019**, *33*, 11101–11112. [[CrossRef](#)]
14. Almeida Streitwieser, D.; Arteaga, A.; Gallo-Cordova, A.; Hidrobo, A.; Ponce, S. Chemical Recycling of Used Motor Oil by Catalytic Cracking with Metal-Doped Aluminum Silicate Catalysts. *Sustainability* **2023**, *15*, 10522. [[CrossRef](#)]

15. Vargas, D.C.; Alvarez, M.B.; Hidrobo Portilla, A.; Van Geem, K.M.; Almeida Streitwieser, D. Kinetic Study of the Thermal and Catalytic Cracking of Waste Motor Oil to Diesel-like Fuels. *Energy Fuels* **2016**, *30*, 9712–9720. [[CrossRef](#)]
16. Rodriguez, Y.; Guerra, R.; Vizuete, K.; Debut, A.; Streitwieser, D.A.; Mora, J.R.; Ponce, S. Kinetic Study of the Catalytic Cracking of Waste Motor Oil Using Biomass-Derived Heterogeneous Catalysts. *Waste Manag.* **2023**, *167*, 46–54. [[CrossRef](#)] [[PubMed](#)]
17. Li, J.; Zhao, P.; Li, T.; Lei, M.; Yan, W.; Ge, S. Pyrolysis Behavior of Hydrochar from Hydrothermal Carbonization of Pinewood Sawdust. *J. Anal. Appl. Pyrolysis* **2020**, *146*, 104771. [[CrossRef](#)]
18. Xiao, L.-P.; Shi, Z.-J.; Xu, F.; Sun, R.-C. Hydrothermal Carbonization of Lignocellulosic Biomass. *Bioresour. Technol.* **2012**, *118*, 619–623. [[CrossRef](#)]
19. Hu, X.; Xu, J.; Wu, M.; Xing, J.; Bi, W.; Wang, K.; Ma, J.; Liu, X. Effects of Biomass Pre-Pyrolysis and Pyrolysis Temperature on Magnetic Biochar Properties. *J. Anal. Appl. Pyrolysis* **2017**, *127*, 196–202. [[CrossRef](#)]
20. Yang, L.; Shuang, E.; Liu, J.; Sheng, K.; Zhang, X. Endogenous Calcium Enriched Hydrochar Catalyst Derived from Water Hyacinth for Glucose Isomerization. *Sci. Total Environ.* **2022**, *807*, 150660. [[CrossRef](#)]
21. Alfredo Quevedo-Amador, R.; Elizabeth Reynel-Avila, H.; Ileana Mendoza-Castillo, D.; Badawi, M.; Bonilla-Petriciolet, A. Functionalized Hydrochar-Based Catalysts for Biodiesel Production via Oil Transesterification: Optimum Preparation Conditions and Performance Assessment. *Fuel* **2022**, *312*, 122731. [[CrossRef](#)]
22. Safari, F.; Javani, N.; Yumurtaci, Z. Hydrogen Production via Supercritical Water Gasification of Almond Shell over Algal and Agricultural Hydrochars as Catalysts. *Int. J. Hydrogen Energy* **2018**, *43*, 1071–1080. [[CrossRef](#)]
23. Meng, S.; Li, W.; Xu, H.; Li, Z.; Li, Y.; Jarvis, J.; Song, H. Non-Thermal Plasma Assisted Catalytic Reforming of Naphtha and Its Model Compounds with Methane at near Ambient Conditions. *Appl. Catal. B* **2021**, *297*, 120459. [[CrossRef](#)]
24. Ardila-Suárez, C.; Pablo Villegas, J.; Lins de Barros Neto, E.; Ghislain, T.; Lavoie, J.-M. Waste Surgical Masks to Fuels via Thermochemical Co-Processing with Waste Motor Oil and Biomass. *Bioresour. Technol.* **2022**, *348*, 126798. [[CrossRef](#)] [[PubMed](#)]
25. Rimez, B.; Breyer, S.; Vekemans, O.; Haut, B. Co-Pyrolysis of Low-Density Polyethylene and Motor Oil—Investigation of the Chemical Interactions between the Components. *Recycling* **2020**, *5*, 33. [[CrossRef](#)]
26. Li, Y.; Hagos, F.M.; Chen, R.; Qian, H.; Mo, C.; Di, J.; Gai, X.; Yang, R.; Pan, G.; Shan, S. Rice Husk Hydrochars from Metal Chloride-Assisted Hydrothermal Carbonization as Biosorbents of Organics from Aqueous Solution. *Bioresour. Bioprocess.* **2021**, *8*, 99. [[CrossRef](#)] [[PubMed](#)]
27. Teng, F.; Zhang, Y.; Wang, D.; Shen, M.; Hu, D. Iron-Modified Rice Husk Hydrochar and Its Immobilization Effect for Pb and Sb in Contaminated Soil. *J. Hazard. Mater.* **2020**, *398*, 122977. [[CrossRef](#)]
28. Naranjo, J.; Juiña, E.; Loyo, C.; Romero, M.; Vizuete, K.; Debut, A.; Ponce, S.; Murillo, H.A. Preparation of Adsorbent Materials from Rice Husk via Hydrothermal Carbonization: Optimization of Operating Conditions and Alkali Activation. *Resources* **2023**, *12*, 145. [[CrossRef](#)]
29. Wathakit, K.; Sukjit, E.; Kaewbuddee, C.; Maithomklang, S.; Klinkaew, N.; Liplap, P.; Arjharn, W.; Srisertpol, J. Characterization and Impact of Waste Plastic Oil in a Variable Compression Ratio Diesel Engine. *Energies* **2021**, *14*, 2230. [[CrossRef](#)]
30. Chen, H.; Wang, X.; Pan, Z. A Comprehensive Study of Fuel Composition, Combustion and Soot Nanostructure Characteristics of a Diesel/Light Hydrocarbons Premixed Charge Compression Ignition Engine. *Fuel* **2020**, *274*, 117858. [[CrossRef](#)]
31. Ying, W.; Longbao, Z.; Hewu, W. Diesel Emission Improvements by the Use of Oxygenated DME/Diesel Blend Fuels. *Atmos. Environ.* **2006**, *40*, 2313–2320. [[CrossRef](#)]
32. ASTM D4809-18; Standard Test Method for Heat of Combustion of Liquid Hydrocarbon Fuels by Bomb Calorimeter (Precision Method). American Society for Testing Materials: West Conshohocken, PA, USA, 2018.

Disclaimer/Publisher’s Note: The statements, opinions and data contained in all publications are solely those of the individual author(s) and contributor(s) and not of MDPI and/or the editor(s). MDPI and/or the editor(s) disclaim responsibility for any injury to people or property resulting from any ideas, methods, instructions or products referred to in the content.